Phys Chem Minerals (2003) 30: 430–439
DOI 10.1007/s00269-003-0334-2

ORIGINAL PAPER

D. G. Isaak · I. Ohno

Elastic constants of chrome-diopside: application of resonant ultrasound spectroscopy to monoclinic single-crystals

Received: 16 September 2002 / Accepted: 2 May 2003

Abstract The right-rectangular parallelepiped resonance (RPR) form of resonant ultrasound spectroscopy (RUS) is applied to monoclinic crystal symmetry to determine the 13 adiabatic elastic constants, C_{ij}, of single-crystal chrome-diopside $Di_{0.93}Hd_{0.03}Ur_{0.02}X_{0.02}$ (Di, diopside; Hd, hedenbergite; Ur, ureyite; X, other or unknown). These data represent the first published values of the elastic tensor for a monoclinic single-crystal determined by the RPR method, thus demonstrating the feasibility of this method for studying elasticity of low-symmetry crystals. The lowest 62 modal frequencies of a gem-quality specimen were measured and identified at ambient temperature and pressure. Inverting the modal frequencies results in, respectively C_{11}, C_{22}, C_{33}, C_{44}, C_{55}, C_{66}, C_{12}, C_{13}, C_{23}, C_{15}, C_{25}, C_{35}, C_{46} values (GPa) of 228.1(1.0), 181.1(0.6), 245.4(1.3), 78.9(0.3), 68.2(0.2), 78.1(0.2), 78.8(0.5), 70.2(0.7), 61.1(0.7), 7.9(0.5), 5.9(0.5), 39.7(0.4), and 6.4(0.2), where numbers in parentheses indicate experimental uncertainty. The corresponding isotropic bulk, K_S, and shear, G, moduli are 116.5 (0.9) and 72.8(0.4) GPa, respectively. When comparing these results with other pyroxene data, we find systematic correlations between M2 site composition and C_{ij} values for most, but not all, moduli. Unusual compositional dependence near end-member diopside is seen for a few moduli, and is propagated to the K_S and G moduli, which should prompt a reexamination of some C_{ij} values of end-member diopside.

D. G. Isaak (✉)
Institute of Geophysics and Planetary Physics,
University of California, Los Angeles,
California, USA
Also at: Department of Mathematics & Physics,
Azusa Pacific University, Azusa, California, USA
e-mail: disaak@apu.edu
Tel.: 310-825-3565
Fax: 310-206-3051

I. Ohno
Department of Earth Sciences,
Faculty of Science, Ehime University,
Bunkyo-cho, Matsuyama, Japan

Keywords Diopside · Clinopyroxene · Elastic constants · Resonant ultrasound spectroscopy · Bulk modulus · Shear modulus

Introduction

Knowledge of the elastic properties of all candidate mantle minerals and how these properties vary with temperature and pressure is required to accurately describe the seismic behavior of Earth's upper and lower mantle. It is generally believed that the four dominant minerals of Earth's upper mantle are olivine, orthopyroxene, clinopyroxene, and pyrope-rich garnet, even though different compositional models ascribe varying amounts of these four minerals to the upper mantle (Weidner 1985; Weidner and Ito 1987; Anderson 1988; Duffy and Anderson 1989; Gwamnesia et al. 1990; Ita and Stixrude 1992; Duffy et al. 1995; Li et al. 1998; Jackson and Rigden 1998). Of these four minerals, olivine has received the most experimental attention, in part because it is considered by most investigators to be the most abundant mineral of Earth's upper mantle. Conversely, clinopyroxene has received relatively little experimental attention even though 15–25% of the uppermost mantle most likely consists of a clinopyroxene component.

Previous measurements of elasticity of monoclinic pyroxene (single crystals) at ambient pressure and temperature include those done on near end members jadeite (Kandelin and Weidner 1988a) and diopside (Levien et al. 1979), as well as omphacite (Bhagat et al. 1992) with composition somewhat intermediate to these end members. These studies all used Brillouin spectroscopy to measure the 13 single-crystal elastic moduli, C_{ij}, of monoclinic pyroxene. Collins and Brown (1998) measured the elastic properties of a natural clinopyroxene, $Di_{72}Hd_9Jd_3Cr_3Ts_{12}$ (Di, diopside; Hd, hedenbergite; Jd, jadeite; Cr, cosmochlor; Ts, Mg-Tschermak) using the impulsive stimulated scattering technique. They illustrate the variation of each C_{ij} along the

diopside–jadeite join by projecting their results on this join and comparing with the three datasets determined by Brillouin spectroscopy. The compositional dependence of C_{ij} along the diopside–jadeite join appears to be irregular for some cases. For moduli C_{11}, C_{55}, and C_{35}, a monotonic change with composition is apparent for all compositions except for end-member diopside. For C_{66} and C_{15}, there is a monotonic change for all four specimens shown on the diopside–jadite join; however, an unusually abrupt change appears near the diopside end-member.

We apply the right-rectangular parallelepiped resonance (RPR) form of resonant ultrasound spectroscopy (RUS) to single-crystal chrome-diopside to obtain its elastic constants. These data represent the first published values of the elastic tensor for a monoclinic single-crystal determined by the RPR method. Our purposes are to: (1) provide elasticity data of single-crystal chrome-diopside at ambient pressure and temperature conditions in order to clarify some features of clinopyroxene elasticity near end member diopside; and (2) demonstrate the application of RPR for monoclinic crystalline symmetry under ambient conditions and anticipated future use at elevated temperature.

Specimen description

A gem-quality natural specimen of chrome-diopside (space group $C2/c$, monoclinic symmetry) was obtained from a commercial source. The specimen is transparent, dark green, and free of any visible inclusions, flaws, or inhomogenities. The elemental composition (Table 1) of the specimen was determined by electron microprobe analysis at five randomly selected spots on a chip cut from the specimen. Well-characterized silicates and oxides were used for standards, in particular, grossular for Si, Al, and Ca, and forsterite for Mg. Table 2 recasts the composition in terms of pyroxene end-member components, yielding $Di_{0.93}Hd_{0.03}Ur_{0.02}X_{0.02}$, where X represents everything other than the known amount of diopside, hedenbergite, and ureyite. The small deviations from perfect stoichiometry are within the collective standard deviations given in Table 1.

Table 1 Chrome-diopside chemical analysis (by element)

Element	Weight percent oxide[a]	Number per six oxygens
Si	56.1(0.2)	2.008
M2 site		
Ca	24.93(0.09)	0.956
Na	0.37(0.04)	0.026
K	0.004(0.006)	0.0002
M1 site		
Mg	17.39(0.08)	0.928
Fe	1.1(0.1)	0.032
Cr	0.84(0.06)	0.024
Al	0.22(0.03)	0.010
Ti	0.07(0.01)	0.0019
Mn	0.046(0.045)	0.0014
Total	101.0	3.987

[a] Numbers in parenthesis are the SD of measurements from five spots

Table 2 Chrome-diopside composition

Pyroxene component	Percent
Diopside (Di), $CaMgSi_2O_6$	93
Hedenbergite (Hd), $CaFe^{+2}Si_2O_6$	3
Ureyite (Ur), $NaCrSi_2O_6$	2
Other, unknown (X)	2[a]

[a] No other single component greater than 1%

We did not test specifically for the Fe^{+2}/Fe^{+3} ratio. However, after combining Ca with Mg to form the dominant end-member diopside, the amount of Ca that remains is very close to the amount of Fe. Thus, practically all Fe is used with Ca to form a hedenbergite component and is, therefore, present as Fe^{+2}.

A right-rectangular parallelepiped was carefully prepared by first orienting and cutting two pairs of opposing faces. The first pair is perpendicular to the [010] axis, which is the two-fold axis, b; the second pair is perpendicular to the [001] axis, which is the c axis. A third pair of faces was cut perpendicular to both of the first two pairs. Since the angle β between the a and c axes is about 106° for diopside, this third pair of faces is not perpendicular to the [100] axis, i.e., the a axis, although it is parallel to the (100) plane. The three pairs of faces were polished to optical quality. The prepared specimen has edge lengths of 4.749 ± 0.002, 4.169 ± 0.003, and 4.905 ± 0.006 mm, with the shortest and longest edges along the [010] and [001] axes, respectively.

The density of the prepared specimen was determined to be 3.286 ± 0.005 g cm^{-3} using an immersion technique with purified water. This measured density is consistent with the range 3.22–3.38 g cm^{-3} for diopside (Deer et al. 1997) and is very near to the value of 3.309 g cm^{-3} given for the chrome diopside in Table 15 (p. 206) of Deer et al. (1997). Differences in amounts of minor contituents such as Al and Cr can account for the small difference in density between our chrome-diopside and that cited by Deer et al. (1997). Indeed, the specimen with density 3.309 g cm^{-3} cited above has about twice the amount of Cr as does our specimen.

Theory of resonant ultrasound spectroscopy applied to monoclinic crystals

The RUS method provides a means to determine the C_{ij} of a single-crystal specimen from measurements of its natural vibrational modes. A type of RUS is RPR, the approach used here, referring to when the specimen has right-rectangular parallelpiped geometry. A specimen's measured resonant spectrum is compared with a calculated spectrum, where the calculated spectrum assumes

initial estimated values for C_{ij}. Since the resonant frequencies of a single-crystal specimen are determined by its density, dimensions, and C_{ij}, the assumed C_{ij} used to calculated the spectrum are adjusted until calculated and measured spectra agree in a least-squares sense. Useful reviews of RUS (and RPR) are found in Maynard (1996), Leisure and Willis (1997), and Migliori and Sarrao (1997).

The application of RPR to single-crystal specimens is based on the theory developed by Demarest (1971) specifically for cube specimens that have isotropic or cubic symmetry. Ohno (1976) extended the theory to more general crystal symmetries, including the monoclinic case; he specifically demonstrated its use in determining the nine elastic constants of single-crystal forsterite, an orthorhombic mineral. Since that time, the RPR technique has been used extensively to determine high-temperature elastic properties of cubic, trigonal, tetragonal, and orthorhombic crystals (see, for example, Anderson and Isaak 1995 and Isaak et al. 1998), but it has not been been applied to lower-symmetry specimens. This last point is emphasized by Schwarz and Vuorinen (2000), albeit an alternative method based on the resonant frequencies of plane-parallel plates (Haussühl et al. 1983) has been used to investigate the C_{ij} of monoclinic crystals (Haussühl 1997; Haussühl et al. 2000).

The application of RPR to monoclinic crystal symmetry has many similarities to trigonal symmetry. We follow Ohno et al.'s (1986) outline for the trigonal case in summarizing the RPR theory as it applies to monclinic crystal symmetry and as used to determine the C_{ij} of chrome-diopside.

The time-independent part of the Lagrangian corresponding to a freely vibrating elastic solid with density ρ can be written as (Demarest 1971):

$$I(\mathbf{u}) = \iiint \sum_i \sum_j \sum_k \sum_l C_{ijkl}\varepsilon_{ij}(\mathbf{u})\varepsilon_{kl}(\mathbf{u})\mathrm{d}v \ , \tag{1}$$

where C_{ijkl} is the elastic constant tensor and $\varepsilon_{ij}(\mathbf{u})$ is the strain tensor defined as

$$\varepsilon_{ij}(\mathbf{u}) = \frac{1}{2}\left(\frac{\partial u_i}{\partial x_j} + \frac{\partial u_j}{\partial x_i}\right) \ , \tag{2}$$

with $\mathbf{u}$ representing the displacement vector (u_i being the x_i component). The integration in Eq. (1) is over the volume of the solid. From Hamilton's principle, the Lagrangian is stationary which implies the time-independent part of the Langrangian represented by Eq. (1) must also be stationary. Thus, we have

$$\delta I(\mathbf{u}) = 0 \ . \tag{3}$$

We apply the Ritz method (Demarest 1971) by representing $\mathbf{u}$ with a series of normalized orthogonal basis functions $\mathbf{v}_p$ having coefficients a_p expressed as

$$\mathbf{u} = \sum_m a_m \mathbf{v}_m \ , \tag{4}$$

where the normalization condition is given by

$$\iiint \sum_i u_i \mathrm{d}v = 1 \ . \tag{5}$$

Defining Γ_{mn} as:

$$\Gamma_{mn} = \iiint \sum_i \sum_j \sum_k \sum_l C_{ijkl}\varepsilon_{ij}(\mathbf{v}_m)\varepsilon_{kl}(\mathbf{v}_n)\mathrm{d}v \ , \tag{6}$$

where $\varepsilon_{ij}(\mathbf{v}_m)$ is the strain tensor corresponding to the basis function $\mathbf{v}_m$, Eqs. (1) and (5) can be expressed as:

$$I = \sum_m \sum_n a_m a_n \Gamma_{mn} \tag{7}$$

and

$$\sum_m a_m^2 = 1 \ . \tag{8}$$

The extremization of Eq. (7) under normalization conditions of Eq. (8) results in the eigenvalue problem (Ohno 1976) of

$$\sum_m a_m(\Gamma_{mn} - \rho\omega^2\delta_{mn}) = 0, \quad \mathrm{n} = 1, 2, \ldots \tag{9}$$

with δ_{mn} defined to be 1 for $m = n$ and 0 otherwise.

Following Ohno et al. (1986), we choose basis functions as the normalized Legendre polynomials, $\bar{P}_\varphi(x_j/l_j)$, where $\bar{P}$ is Legendre polynomial of degree φ and $2l_j$ is the edge length in the jth direction, so that

$$\begin{aligned} \mathbf{v}_m &= \frac{1}{\sqrt{l_1 l_2 l_3}}\bar{P}_\lambda(x_1/l_1)\bar{P}_\mu(x_2/l_2)\bar{P}_\nu(x_3/l_3)\mathbf{e}_i \\ \mathbf{v}_n &= \frac{1}{\sqrt{l_1 l_2 l_3}}\bar{P}_\xi(x_1/l_1)\bar{P}_\zeta(x_2/l_2)\bar{P}_\eta(x_3/l_3)\mathbf{e}_j \ , \end{aligned} \tag{10}$$

with $\mathbf{e}_i$ and $\mathbf{e}_j$ indicating unit vectors in the x_i and x_j directions. In Eq. (10), the leading multiplicative term normalizes the expression, and each combination of λ, μ, and ν, or ξ, ζ, and η designates a separate m or n, respectively.

Development of the Γ matrix in Eq. (6) is simplified somewhat by the form of the C_{ijkl} tensor. Utilizing the usual two-suffix notation in place of the four-suffix tensor form, i.e., $11 \to 1$, $22 \to 2$, $33 \to 3$, 23 and $32 \to 4$, 13 and $31 \to 5$, and 12 and $21 \to 6$, and recalling that $C_{ij} = C_{ji}$, we write the monoclinic elastic constant tensor using standard orientation with x_2 having twofold symmetry as

$$C_{ij} = \begin{pmatrix} C_{11} & C_{12} & C_{13} & 0 & C_{15} & 0 \\ & C_{22} & C_{23} & 0 & C_{25} & 0 \\ & & C_{33} & 0 & C_{35} & 0 \\ & & & C_{44} & 0 & C_{46} \\ & & & & C_{55} & 0 \\ & & & & & C_{66} \end{pmatrix} \tag{11}$$

For a basis set in Eq. (4) with N terms, the Γ matrix is a symmetric $3N \times 3N$ matrix which can be broken into nine $N \times N$ sections. Each section corresponds to i,j = 1,1; 1,2; 1,3; 2,1; 2,2; 2,3; 3,1; 3,2; and 3,3. Working out terms for the required six unique cases of i,j in con-

structing the elements of Γ_{mn} for monoclinic crystals gives:

$$\begin{cases} (i,j) & \Gamma_{mn} \\ (1,1) & C_{11}G_1 + C_{66}G_2 + C_{55}G_3 + C_{15}G_6 + C_{15}G_7 \\ (2,2) & C_{66}G_1 + C_{22}G_2 + C_{44}G_3 + C_{46}G_6 + C_{46}G_7 \\ (3,3) & C_{55}G_1 + C_{44}G_2 + C_{33}G_3 + C_{35}G_6 + C_{35}G_7 \\ (2,3) & C_{44}G_4 + C_{23}G_5 + C_{25}G_8 + C_{46}G_9 \\ (3,1) & C_{15}G_1 + C_{46}G_2 + C_{35}G_3 + C_{55}G_6 + C_{13}G_7 \\ (2,3) & C_{25}G_4 + C_{46}G_5 + C_{66}G_8 + C_{12}G_9 \end{cases} \tag{12}$$

where

$$\begin{cases} G_1 = D_{\lambda\xi}\delta_{\mu\zeta}\delta_{\nu\eta}/l_1^2 & G_2 = \delta_{\lambda\xi}D_{\mu\zeta}\delta_{\nu\eta}/l_2^2 & G_3 = \delta_{\lambda\xi}\delta_{\mu\zeta}D_{\nu\eta}/l_3^2 \\ G_4 = \delta_{\lambda\xi}E_{\mu\zeta}E_{\eta\nu}/l_2 l_3 & G_5 = \delta_{\lambda\xi}E_{\zeta\mu}E_{\nu\eta}/l_2 l_3 & G_6 = E_{\xi\lambda}\delta_{\mu\zeta}E_{\nu\eta}/l_3 l_1 \\ G_7 = E_{\lambda\xi}\delta_{\mu\zeta}E_{\eta\nu}/l_3 l_1 & G_8 = E_{\lambda\xi}E_{\zeta\mu}\delta_{\nu\zeta\eta}/l_1 l_2 & G_9 = E_{\xi\lambda}E_{\mu\zeta}\delta_{\nu\eta}/l_1 l_2 \end{cases} \tag{13}$$

and

$$\begin{cases} \delta_{\lambda\xi} = 1, \text{ for } \lambda = \xi \\ \delta_{\lambda\xi} = 0, \text{ for } \lambda \neq \xi \\ E_{\lambda\xi} = \sqrt{(2\lambda+1)(2\xi+1)}, \text{ for } \lambda < \xi \text{ and } \lambda+\xi \text{ odd}, \\ E_{\lambda\xi} = 0, \text{otherwise} \\ \text{for } (\lambda \geq \xi) \\ D_{\lambda\xi} = D_{\xi\lambda} = \sqrt{(2\lambda+1)(2\xi+1)}(\xi+1)\xi/2, \text{ for } \lambda+\xi \text{ even} \\ D_{\lambda\xi} = 0, \text{ for } \lambda+\xi \text{ odd}. \end{cases} \tag{14}$$

The Γ matrix can be split into zero and nonzero components (see Sect. 2.4 in Ohno et al. 1976), which simplifies the calculations considerably. This splitting requires parity considerations connecting the symmetry of the elastic constants with the symmetry of the prepared specimen. The twofold rotation $C_2(y)$, mirror reflection $\sigma(xz)$, inverson i, and identity operation E are symmetry operations common to both the elastic constants and the prepared right-rectangular parallelepiped specimen, forming the point group C_{2h}. Ohno et al. (1986) show that point group C_{2h} has four possible types of displacements. These four displacement types are called mode groups and labeled Ag, Au, Bg, and Bu according to standard group theory convention. In this convention, A denotes symmetric and B antisymmetric, both with respect to $C_2(y)$, and g represents gerade and u ungerade, both with respect to i. The nth vibrational mode of Ag, for example, is then designated by Ag-n. Table 3 summarizes the characteristics of the four modes groups with respect to the symmetry operations of point group C_{2h}.

In the monoclinic situation where the y-axis is the twofold axis, the ensuing parity of displacement components u_1, u_2, u_3 are listed in Table 4. When basis functions described by Eq. (10) are used, we must choose Legendre polynomials as given in Table 4 which ensures that properties listed in Table 3 are met. Every Γ_{mn} in Eq. (6) vanishes for pairs of basis functions belonging to different mode groups, allowing the Γ matrix to be factored into four smaller matrices. The eigenvalues of each of the four smaller matrices can be separately calculated.

The calculated eigenvalues give the frequencies f_n used to identify the mode type of each measured modal

Table 3 Characteristics of four modes groups with respect to symmetry operations for point group C_{2h} with y-axis parallel to the twofold axis

Mode group	E	$C_2(y)$	i	$\sigma(xz)$
Ag	1	1	1	1
Au	1	1	−1	−1
Bg	1	−1	1	−1
Bu	1	−1	−1	1

Table 4 Parity (E even; O odd) of degrees of the Legendre polynomials in the basis functions in Eq. (10)

Mode group	Displacement	μ (ζ)	$\lambda+\nu$ ($\xi+\eta$)
Ag	u_1	E	O
	u_2	O	E
	u_3	E	O
Au	u_1	O	O
	u_2	E	E
	u_3	O	O
Bg	u_1	O	E
	u_2	E	O
	u_3	O	E
Bu	u_1	E	E
	u_2	O	O
	u_3	E	E

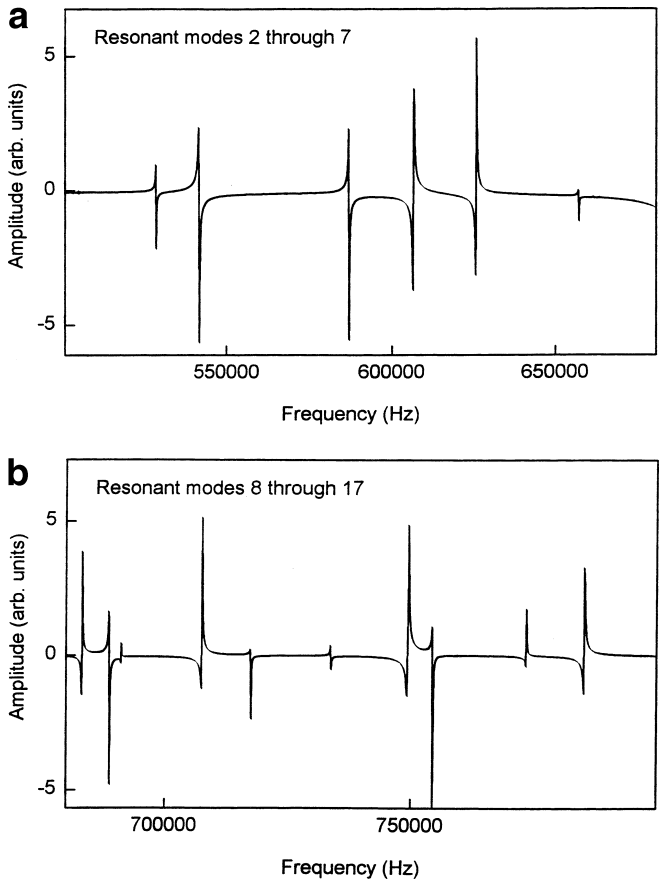

Fig. 1a, b Sample of measured spectrum for chrome-diopside specimen used in this study. The resonant frequencies shown are for modes **a** 2–7 and **b** 8–17

frequency. The elastic constants can then be determined from standard inverse procedures as summarized in Sec. 3.3 of Ohno (1976). The values of $\partial f_n/\partial C_{ij}$ required in the inversion are determined by the method described by Oda et al. (1993).

Experimental procedures

The prepared specimen was placed between a pair of small disk-shaped ceramic transducers. The transducer diameters are about 2 mm. One transducer provides mechanical vibration to the specimen; the other transducer monitors the vibrational amplitude of the specimen. By scanning a range of frequencies, a spectrum of vibrational resonances of the specimen is obtained. We scanned the chrome-diopside specimen using the Dynamic Resonance Systems, Inc. (DRS) modulus apparatus.

While obtaining resonance spectra, the transducer-specimen couplings were done by lightly touching the transducers to opposite faces of the specimen. This differs from our past practice of coupling larger transducers to the specimen at the specimen corners (Goto and Anderson 1988; Isaak et al. 1989; Ohno 1990) in order to obtain good signal-to-noise. We found that an excellent resonance signal is obtained with the small transducers used here when touching them to opposing faces of the specimen.

Table 5 Measured and calculated spectra of first 62 modal frequencies

Mode	f_{meas} (kHz)	f_{calc} (kHz)	Δf^a (%)
A*u*-01	397.1	396.4	0.2
A*u*-02	528.3	527.9	0.1
A*g*-01	541.6	541.6	< 0.1
B*u*-01	587.0	585.4	0.3
A*u*-03	606.7	606.8	< −0.1
B*u*-02	625.9	627.4	−0.2
B*g*-01	657.1	656.8	0.1
A*u*-04	683.3	683.5	< −0.1
B*g*-02	688.8	689.1	< −0.1
A*g*-02	691.2	691.4	< −0.1
A*g*-03	707.8	707.4	0.1
B*u*-03	718.0	718.4	< −0.1
B*g*-03	733.8	734.6	−0.1
A*g*-04	749.5	749.7	< −0.1
B*u*-04	754.7	753.9	0.1
B*g*-04	773.8	772.9	0.1
A*g*-05	785.3	784.6	< 0.1
A*g*-06	826.7	826.6	< 0.1
B*g*-05	834.7	834.4	< 0.1
B*u*-05	860.3	861.3	−0.1
A*g*-07	866.1	865.2	0.1
A*u*-05	893.0	892.7	< 0.1
B*u*-06	899.3	898.9	< 0.1
B*g*-06	900.9	900.3	< 0.1
A*u*-06	926.0	925.3	< 0.1
B*u*-07	932.5	934.7	−0.2
A*g*-08	972.3	972.1	< 0.1
B*u*-08	1007.0	1006.5	< 0.1
B*u*-09	1026.4	1027.1	< −0.1
A*g*-09	1034.8	1034.6	< 0.1
A*u*-07	1036.3	1037.4	< −0.1
A*u*-08	1066.4	1066.3	< 0.1
B*u*-10	1080.3	1080.7	< −0.1
A*g*-10	1090.5	1090.4	< 0.1
A*g*-11	1095.9	1095.6	< 0.1
A*u*-09	1096.4	1097.5	−0.1
B*g*-07	1141.6	1142.1	< −0.1
A*u*-10	1168.9	1166.3	0.2
B*g*-08	1165.9	1167.9	−0.2
B*g*-09	1191.7	1191.7	< 0.1
A*g*-12	1193.9	1194.1	< −0.1
B*u*-11	1199.3	1197.5	0.1
B*g*-10	1214.8	1214.3	< 0.1
B*u*-12	1226.6	1227.1	< −0.1
B*u*-13	1240.3	1239.2	< 0.1
A*g*-13	1251.8	1252.4	< −0.1
A*u*-11	1266.8	1265.9	< 0.1
B*u*-14	1280.1	1280.9	< −0.1
A*g*-14	1282.8	1282.8	< 0.1
A*u*-12	1294.4	1295.0	< −0.1
B*g*-11	1301.7	1302.1	< −0.1
A*g*-15	1315.7	1316.8	< −0.1
A*u*-13	1346.3	1346.6	< −0.1
A*g*-16	1354.2	1355.3	< −0.1
A*u*-14	1355.8	1357.1	< −0.1
B*g*-12	1361.6	1362.1	< −0.1
B*u*-15	1382.1	1382.6	< −0.1
B*g*-13	1384.4	1383.4	< 0.1
A*u*-15	1389.0	1388.8	< 0.1
B*u*-16	1403.4	1401.3	0.1
B*g*-14	1401.4	1402.0	< −0.1
A*g*-17	1411.2	1411.2	< 0.1

[a] $\frac{f_{meas}-f_{calc}}{f_{meas}} \times 100$

Table 6 Single-crystal elastic moduli (GPa) of some clinopyroxene materials

Elastic modulus	Chrome-diopside[a]	Diopside[b]	Hedenbergite[c]	$Di_{72}Hd_9Jd_3Cr_3Ts_{12}$[d]
C_{11}	228.1 ± 1.0	223 ± 2	222 ± 6	237.8 ± 0.8
C_{22}	181.1 ± 0.6	171 ± 2	176 ± 5	183.6 ± 0.9
C_{33}	245.4 ± 1.3	235 ± 2	249 ± 5	229.5 ± 0.9
C_{44}	78.9 ± 0.3	74 ± 1	55 ± 3	76.5 ± 0.9
C_{55}	68.2 ± 0.2	67 ± 1	63 ± 2	73.0 ± 0.4
C_{66}	78.1 ± 0.2	66 ± 2	60 ± 4	81.6 ± 1.0
C_{12}	78.8 ± 0.5	77 ± 3	69 ± 14	83.5 ± 1.3
C_{13}	70.2 ± 0.7	81 ± 2	79 ± 9	80.0 ± 1.1
C_{23}	61.1 ± 0.7	57 ± 2	86 ± 10	59.9 ± 1.6
C_{15}	7.9 ± 0.5	17 ± 1	12 ± 3	9.0 ± 0.6
C_{25}	5.9 ± 0.5	7 ± 2	13 ± 7	9.5 ± 1.0
C_{35}	39.7 ± 0.4	43 ± 1	26 ± 3	48.1 ± 0.6
C_{46}	6.4 ± 0.2	7.3 ± 0.9	−10 ± 3	8.4 ± 0.8
[e]K_S	116.5 ± 0.9	113	120	117.2 ± 0.7
[f]G	72.8 ± 0.4	67.0	61	72.2 ± 0.2

[a] Current results;
[b] Levien et al. (1979);
[c] Kandelin and Weidner (1988b);
[d] Collins and Brown (1998);
[e] Isotropic bulk modulus;
[f] Isotropic shear modulus

We observed 62 resonance modes at ambient pressure and temperature (~24 °C) using about 5 g-wt (0.049 N) of holding force coupling the transducers to the specimen. Figure 1a and b depicts modes 2–17 of the measured spectrum and illustrates the excellent signal that was obtained. The nonsymmetrical or, in some cases, inverted appearance of these modes results from phase shifts between the resonant signal and coherent background noise, including electromagnetic and mechanical pickup. The DRS apparatus is equipped to phase shift the measured spectrum so as to produce Lorentzian-like peaks from the raw spectrum. However, applying these phase shifts resulted in barely noticeable changes in the value of the resonant frequency compared to those estimated from the raw spectrum, a result that is expected when the dissipation is relatively low (Migliori and Sarrao 1997).

The RPR theory assumes a freely vibrating specimen; thus, we must consider to what extent the transducer-specimen holding force alters the measured resonances from that of a specimen with no boundary constraints. We reduced the holding force to less than 1 g-wt (0.0098 N), so that a signal was barely perceptible for 31 of the 62 modes. No signal was seen for the remaining 31 modes under these conditions. For 26 of the 31 modes observed at the reduced holding force, the measured resonances shifted by 0.1 kHz, or less, when comparing with the data from 5 g-wt of holding force. Four modes shifted by 0.2 kHz and one by 0.3 kHz. A temperature change of 1 °C corresponds to a frequency shift of about 0.1 kHz. Thus, the overall uncertainty in frequency due to a nonzero holding force corresponds to an uncertainty in ambient temperature of approximately 1 °C.

In the RPR technique, inversion of the frequency spectrum requires mode assignment of the measured spectrum. We initially attempted mode assignment by comparing the measured spectrum with that calculated from diopside elasticity data from Levien et al. (1979). However, several ambiguities surfaced when trying to align modes. These ambiguities are related to three problematic C_{ij} described in the Discussion section. When we used the C_{ij} data of Collins and Brown (1998), however, we found obvious alignment of 43 modes when comparing between our measured and the calculated spectra. Using this initial identification of 43 modes, we eventually determined C_{ij} consistent with all 62 measured modes.

Results

We determined the 13 adiabatic elastic constants of the chrome-diopside specimen at ambient temperature from the measured spectrum of the first 62 modal frequencies. Table 5 lists each of these 62 modes along with their measured values, f_{meas}. The converged set of C_{ij} determined from the modes given in Table 5 is listed in Table 6. Included in Table 6 are the respective isotropic bulk and shear moduli, K_S and G. These isotropic moduli are the average of the Voigt and Reuss bounds; which, for diopside, are coincident with the arithmetic means of the Hashin–Shtrikman bounds (Watt 1980).

The data are self-consistent, as seen by comparing the modal frequencies calculated from the final set of C_{ij} (f_{calc} in Table 5) with the measured spectrum. This self-consistency provides confirmation that our initial mode assignment is correct. Given the initial mode assignment, reasonable alternative sets of starting C_{ij}, such as the values reported by Levien et al. (1979), converge to our same final values.

We used the Ohno (1976) reduction scheme for inverting the frequency data to obtain the C_{ij}. Almost five times as many modal frequencies (62) were measured as the number of elastic constants (13) to be determined. Many modes, however, provide much stronger constraints on shear, instead of compressional, moduli (Migliori and Sarrao 1997). In the Ohno (1976) scheme, this problem appears as similarities in the ratio of the $\partial f_n/\partial C_{ij}$ vectors for different C_{ij}. So, the situation is not as overdetermined as first appears, and using only the RMS of the residuals of the fitted frequencies does not provide a secure measure of the uncertainties in the final set of computed C_{ij}, especially the compressional moduli.

We use the square root of the diagonal elements of the error matrix (Bevington and Robinson 1992) for determining uncertainties in the C_{ij} due to standard deviations of the fitted frequencies. This error matrix is the $(T^tT)^{-1}$ matrix of Eq. (25) in Ohno (1976) times the RMS of the residuals. Ultimately, similarities in the $\partial f_n/\partial C_{ij}$ vectors result in the T^tT matrix tending to be ill-conditioned, and the error estimates on the C_{ij} grow accordingly. Thus, our error estimates due to the standard deviations of the fitted frequencies are influenced by similarities in the ratio of the $\partial f_n/\partial C_{ij}$ vectors for different C_{ij} as well as the overall goodness of the frequency fit.

The final uncertainty for each of the single-crystal C_{ij} tensor components listed in Table 6 is fully propagated

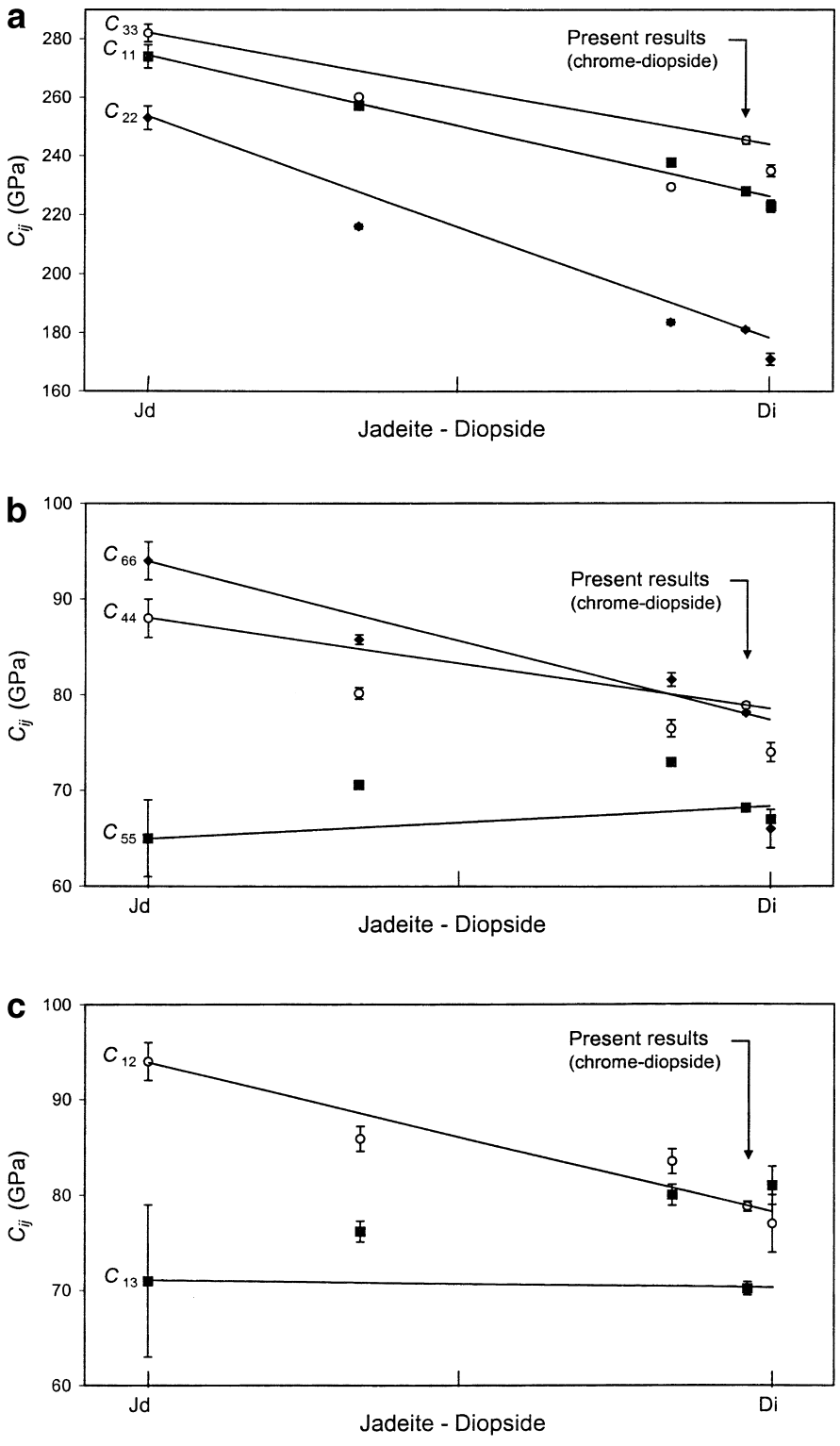

Fig. 2a–e The variation of: **a** C_{11}, C_{22}, and C_{33}; **b** C_{44}, C_{55}, and C_{66}; **c** C_{12} and C_{13}; **d** C_{23} and C_{35}; and **e** C_{15}, C_{25}, and C_{46} with composition. Sources of data and nominal Di/(Di + Jd) ratios are: Kandelin and Weidner (1988a) 0.0; Bhagat et al. (1992) 0.341; Collins and Brown (1998) 0.84; chrome-diopside 0.96; and Levian et al. (1979) 1.0. The M2-site ratio Ca/(Ca + Na) ≈ 0.96 for chrome-diopside, fixing the nominal Di/(Di + Jd) as 0.96. *Lines* originate at jadeite end member and extend through chrome-diopside data

from three effects: (1) the standard deviations of the fitted frequencies discussed above; (2) the stated uncertainties in ρ; and (3) the stated uncertainty in specimen edge lengths. The standard deviations of the fitted frequencies are the largest effect, making 75%, or more, of each listed uncertainty for C_{ij} in Table 6. The errors for K_S and G are fixed by considering contributions from both the width of the Hashin–Shtrikman bounds (H^- to H^+ being about 1.7 GPa for diopside: Watt 1980) and estimating uncertainty in the placement of the bounds due to error in the individual C_{ij}. The former is the dominant effect.

Fig. 2a–e (Contd.)

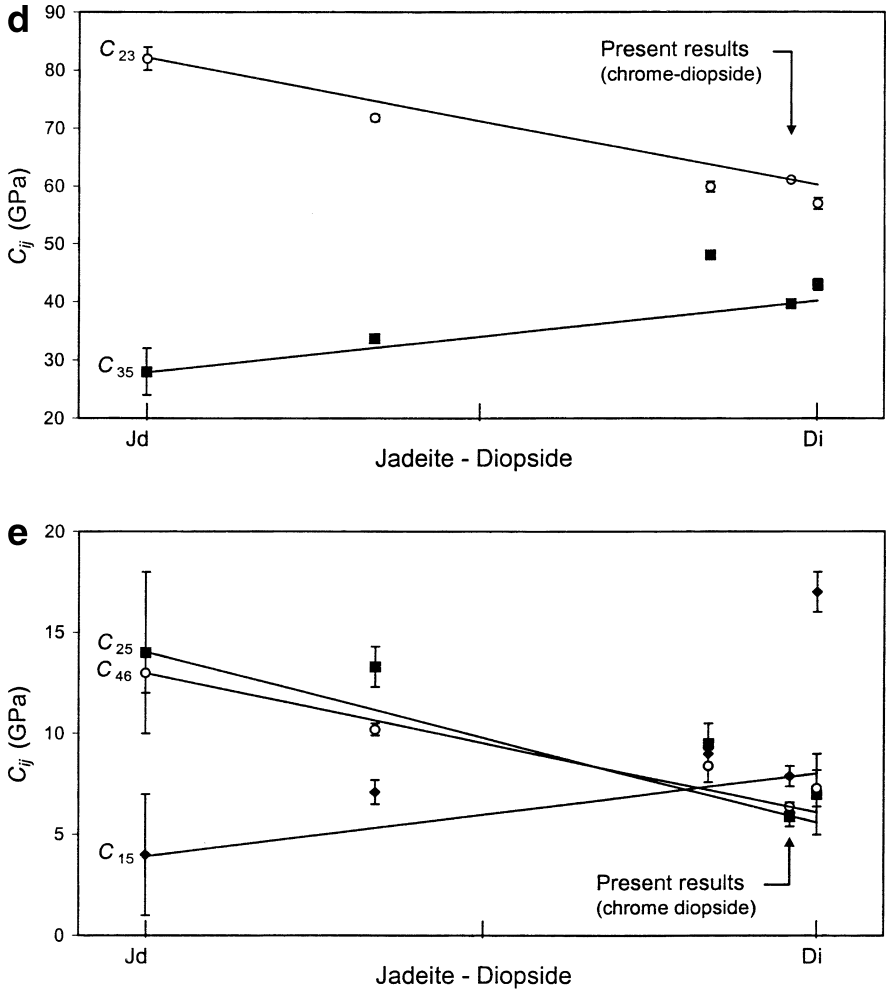

Discussion

Since our chrome-diopside specimen is 93% diopside and only 3% hedenbergite, it is reasonable to expect that the measured C_{ij} will be near those found by Levien et al. (1979) for near-end-member diopside (see Table 6). (The Levien et al. 1979 specimen has composition $Ca_{0.99}Na_{0.02}Mg_{0.98}Al_{0.01}Fe_{0.02}Si_{1.99}O_6$ which we call end-member diopside hereafter without further qualification.) The values for C_{11}, C_{55}, C_{12}, C_{25}, and C_{46} are each within 1% of the respective C_{ij} reported by Levien et al. (1979) when experimental uncertainties are taken into account. The C_{44}, C_{23}, and C_{35} deviate by more than 1% from end-member diopside, but the chrome-diopside and diopside values for these three moduli are still relatively close to each other compared to their hedenbergite counterparts in Table 6.

Among the five remaining C_{ij}, three appear problematic. The percent differences between the chrome-diopside and diopside C_{66}, C_{13}, and C_{15} moduli are 15, 15, and 115%, respectively. Further, the chrome-diopside values are not intermediate to diopside and hedenbergite for these moduli, pointing to causes other than the 3% hedenbergite component in our chrome-diopside for their origin. If these differences in C_{ij} are due to compositional differences only, it must be that some C_{ij} are very sensitive to small amounts of Cr and/or Na.

Bhagat et al. (1992) note that estimates of elastic moduli can be made by considering the mole fractions of diopside to jadeite along the Di–Jd join. Collins and Brown (1998) followed Bhagat et al. (1992) and recast their natural clinopyroxene $Di_{72}Hd_9Jd_3Cr_3Ts_{12}$ in terms of $(Di + Hd)_{84}(Jd + Ts)_{16}$, placing their data on the $Di_{84}Jd_{16}$ point of the Di–Jd join. Collins and Brown point out that this approach assumes that the large atom in the M2 site controls variations in the elastic moduli along the Di–Jd join.

Our chrome-diopside specimen has M2 occupied by Ca (96%) and Na (3%), with 1% unknown. Thus, the Ca/(Ca + Na) ratio in the M2 site is very near to 0.96, and we consider our specimen to be 96% diopside-like, with the remaining 4% jadeite-like. Comparisons between our results and C_{ij} data on the Di–Jd join are obtained by placing our data at an assumed value of 0.96 for Di:Jd. We emphasize that even though our specimen does not contain significant amounts of jadeite, we use its Ca/(Ca + Na) ratio (M2 site atoms) to compare our results with other pyroxenes on the Di–Jd join. Fig-

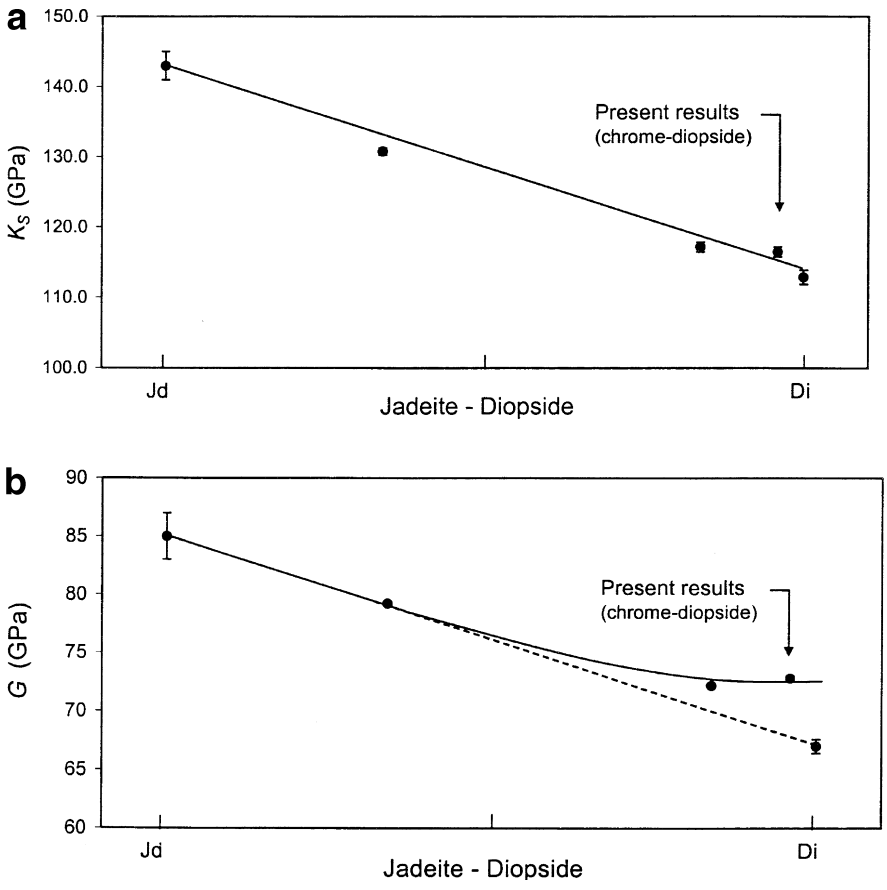

Fig. 3a, b The variation of the isotropic moduli **a** K_S, and **b** G with composition. Sources of data and nominal Di/(Di + Jd) ratios are: Kandelin and Weidner (1988a) 0.0; Bhagat et al. (1992) 0.341; Collins and Brown (1998) 0.84; present chrome-diopside, 0.96; and Levien et al. (1979) 1.0. The M2-site ratio Ca/(Ca + Na)≈ 0.96 for chrome-diopside, fixing the nominal Di/(Di + Jd) as 0.96. The chrome-diopside K_S and G are calculated from C_{ij} in Table 4

ure 2a–e shows the 13 elastic moduli obtained for nominal Di:Jd ratios of 0.0 (Kandelin and Weidner 1988a), 0.341 (Bhagat et al. 1992), 0.84 (Collins and Brown 1998), 0.96 (current results), and 1.0 (Levien et al. 1979). In Fig. 2a–e, we connected the end-member jadeite C_{ij} to the chrome-diopside data presented here.

Trends seen in Fig. 2a–e are systematic for most, but not all, moduli. Inspection of Fig. 2b–d illustrates the unusual compositional dependence near diopside end member for C_{66}, C_{13}, and especially C_{15} mentioned above. We emphasize, however, that the comparisons shown in Fig. 2a–e are only to illustrate general trends, since intermediate compounds in these plots do not belong exactly on the Di:Jd join. Further, our value for the C_{13} modulus appears to deviate from the trend. It is possible that some C_{ij} are unusually sensitive to small compositional changes in the M2 site or to compositional differences in the M1 site; this latter consideration is unaccounted for entirely when placing the intermediate compounds on the Di:Jd join in Fig. 2a–e.

In Fig. 3a and b, compositional trends in the computed isotropic bulk, K_S, and shear, G, moduli are illustrated. The isotropic moduli of our data are the average of the Hashin–Shtrikman upper and lower bounds as described by Watt (1980). Figure 3b reveals little variation in K_S and especially G with composition when comparing the chrome-diopside and the Collins and Brown (1998) result even though their specimen has 12% $MgAl(AlSi)O_6$ Mg-tschermak. This insensitivity to composition does not continue with further changes in composition to end-member diopside.

We emphasize that there are relatively small compositional difference between chrome-diopside and diopside, but the chrome-diopside value for G is 8% higher than for diopside. This seems problematic. Our chrome-diopside has a few percent hedenbergite, but hedenbergite (see Table 6) has a lower G than does diopside. Therefore, we are left with only the 2% ureyite (chrome and sodium components) in chrome-diopside, if we are to explain the higher value of G in the chrome-diopside G in terms of compositional differences. This explanation requires an unusually strong depedence of C_{ij} on minor components. A reexamination of the end-member diopside C_{ij} is warranted to confirm this prospect.

Conclusion

The RPR form of the resonant ultrasound RUS method is successfully applied to single-crystal chrome-diopside in determining the 13 independent C_{ij} of this monoclinic material. These results represent the first published values of the elastic tensor for a monoclinic single-crystal determined with RPR, demonstrating that RPR can be an effective tool for studying the elastic properties of low-symmetry crystals.

The lowest 62 resonant modes of a gem-quality specimen were measured and identified. We obtain excellent correspondence between all 62 measured frequencies with those calculated from our final set of C_{ij}. This correspondence between calculated and measured frequencies results in relatively small errors in the C_{ij} determined here, and gives confidence that our mode identification is accurate.

Systematic trends are observed for most, but not all, C_{ij} when comparing with other pyroxene data by projecting on to the Di:Jd join. Unusual compositional dependence near the diopside end member is seen with C_{66}, C_{13}, and C_{15}, and propagate to the shear modulus G. Reasons for this unusual behavior are not altogether clear, but they are most likely related, in part, to compositional variations in both M2 and M1 sites not considered when projecting the data onto the Di:Jd join.

We find most C_{ij} are within a percent, or so, of those reported on end-member diopside (Levien et al. 1979). Of special note and concern, however, are the relatively large differences between C_{66}, C_{13}, C_{15}, and G when comparing the new chrome-diopside data with diopside, given their similar compositions. These considerations indicate that experimental investigation of some C_{ij} of end-member diopside warrant revisiting.

Acknowledgements CAMET Research, Inc. (Santa Barbara, California) performed specimen orientation. Steven Moser assisted in the sample preparation. Wayne Dollase (UCLA) provided valuble suggestions, including careful reviews of this manuscript, as did Baosheng Li and one other anonymous reviewer. This research was supported by NSF EAR-0073989. IGPP No. 5766.

References

Anderson DL (1988) Temperature and pressure derivatives of elastic constants with application to the mantle. J Geophys Res 93: 4688–4700

Anderson OL, Isaak DG (1995) Elastic constants of mantle minerals at high temperature. In: Ahrens TJ (ed) Mineral physics and crystallography, a handbook of physical constants (AGU Ref Shelf 2) American Geophysical Union, Washington, DC

Bevington PR, Robinson DK (1992) Data reduction and error analysis for the physical sciences. McGraw-Hill, New York

Bhagat SS, Bass JD, Smyth JR (1992) Single-crystal elastic properties of omphacite-$C2/c$ by Brillouin spectroscopy. J Geophys Res 97: 6843–6848

Collins MD, Brown JM (1998) Elasticity of an upper mantle clinopyroxene. Phys Chem Miner 26: 7–13

Deer WA, Howie RA, Zussman J (1997) Rock-forming minerals, vol 2A. Single-chain silicates (2nd ed.). Geological Society, London

Demarest Jr HH (1971) Cube-resonance method to determine the elastic constants of solids. J Acoust Soc Am 49: 768–774

Duffy T, Anderson DL (1989) Seismic velocities in mantle minerals. J Geophys Res 94: 1895–1912

Duffy TS, Zha C, Downs RT, Mao HK, Hemley RJ (1995) Elasticity of forsterite to 16 GPa and the composition of the upper mantle. Nature 378: 170–173

Goto T, Anderson OL (1988) Apparatus for measuring elastic constants of single crystals by a resonance technique up to 1825 K. Rev Sci Instrum 59: 1405–1408

Gwanmesia GD, Rigden SM, Jackson I, Liebermann RC (1990) Pressure dependence of elastic wave velocity for β-Mg_2SiO_4 and the composition of Earth's mantle. Science 250: 794–797

Haussühl S (1983) Kristallphysik. Physik-Verlag Chemie, Weinheim

Haussühl S (1997) Elastic properties of sulfanilates of Li, Na, K, Rb, Cs, Tl, NH_4, CH_3NH_3 and $C(NH_2)_3$. Z Kristallogr 212: 186–190

Haussühl S, Kutzke H, Klapper H (2000) Physical properties of stable monoclinic and metastable trigonal 4-methylbenzophenone. Z Kristallogr 215: 187–189

Isaak DG, Anderson OL, Goto T, Suzuki I (1989) Elasticity of single-crystal forsterite measured to 1700 K. J Geophys Res 94: 5895–5906

Isaak DG, Carnes JD, Anderson OL, Cynn H, Hake E (1998) Elasticity of TiO_2 rutile to 1800 K. Phys Chem Miner 26: 31–43

Ita J, Stixrude L (1992) Petrology, elasticity, and composition of the mantle transition zone. J Geophys Res 97: 6849–6866

Jackson I, Rigden SM (1998) Composition and temperature of the Earth's mantle: Seismological models interpreted through experimental studies of Earth materials, In: Jackson I (ed) The Earth's mantle: composition, structure, and evolution. Cambridge University Press, New York

Kandelin J, Weidner DJ (1988a) The single-crystal elastic properties of jadeite. Phys Earth Planet Int 50: 251–260

Kandelin J, Weidner DJ (1988b) Elastic properties of hedenbergite. J Geophys Res 93: 1063–1072

Leisure RG, Willis FA (1997) Resonant ultrasound spectroscopy. J Phys Condens Matter 9: 6001–6029

Levien L, Weidner DJ, Prewitt CT (1979) Elasticity of diopside. Phys Chem Miner 4: 105–113

Li B, Liebermann RC, Weidner DJ (1998) Elastic moduli of wadsleyite (β-Mg_2SiO_4) to 7 Gigapascals and 873 Kelvin. Science 281: 675–677

Maynard J (1996) Resonant ultrasound spectroscopy. Phys Today 49: 26–29

Migliori A, Sarrao JL (1997) Resonant ultrasound spectroscopy. Wiley, New York

Oda H, Suzuki I, Ohno I (1993) Partial derivatives of eigenfrequencies of a rectangular parallelepiped and a sphere of elastically anisotropic solid. J Phys Earth 41: 271–289

Ohno I (1976) Free vibration of a rectangular parallelepiped crystal and its application to determinatin of elastic constants of orthorhombic crystals. J Phys Earth 24: 355–379

Ohno I (1990) Rectangular parallelepiped resonance method for piezoelectric crystals and elastic constants of alpha-quartz. Phys Chem Miner 17: 371–378

Ohno I, Yamamoto S, Anderson OL, Noda J (1986) Determination of elastic constants of trigonal crystals by the rectangular parallelepiped resonance method. J Phys Chem Solids 47: 1103–1108

Schwarz RB, Vuorinen JF (2000) Resonant ultrasound spectroscopy: applications, current status and limitations. J Alloys Compounds 310: 243–250

Watt JP (1980) Hashin–Shtrikman bounds on the effective elastic moduli of crystals with monoclinic symmetry. J Appl Phys 51: 1520–1524

Weidner DJ (1985) A mineral physics test of a pyrolite mantle. Geophys Res Lett 12:417–420

Weidner DJ, Ito E (1987) Mineral physics contraints on a uniform mantle composition. In: Manghnani MH, Syono Y (eds) High-pressure research in mineral physics. American Geophysical Union, Washington, DC